The Astrophysical Journal, 888:123 (7pp), 2020 January 10 https://doi.org/10.3847/1538-4357/ab5dc9


# Precision of Mass and Radius Determination for Neutron Stars from the *ATHENA* Mission

Agnieszka Majczyna[1], Jerzy Madej[2], Mirosław Należyty[2], Agata Różańska[3], and Bartosz Bełdycki[3]
[1] National Centre for Nuclear Research, ul. Andrzeja Sołtana 7, 05-400 Otwock, Poland; agnieszka.majczyna@ncbj.gov.pl
[2] Astronomical Observatory, University of Warsaw, Al. Ujazdowskie 4, 00-478 Warszawa, Poland
[3] Nicolaus Copernicus Astronomical Centre, Polish Academy of Sciences, ul. Bartycka 18, 00-716 Warszawa, Poland
*Received 2019 February 28; revised 2019 November 4; accepted 2019 November 26; published 2020 January 16*

## Abstract

In this paper we show that X-ray spectral observations of the *ATHENA* mission, which is planned to launch in 2031, can constrain the equation of state (EOS) of superdense matter. We use our well-constrained continuum-fitting method to determine the mass and radius of a neutron star. Model spectra of the emission from a neutron star were calculated using the atmosphere code ATM24. In the next step, those models were fitted to simulated spectra of the neutron star calculated for *ATHENA*'s Wide Field Imager (WFI) detector, using satellite calibration files. To simulate the spectra we assumed three different values of effective temperature, surface gravity, and gravitational redshift. These cases relate to three different neutron star masses and radii. This analysis allows us to demonstrate both the precision of our method and the need for a fast detector onboard *ATHENA*. A large grid of theoretical spectra was calculated with various parameters and a hydrogen–helium–iron composition of solar proportions. These spectra were fitted to the simulated spectrum to estimate the precision of mass and radius determination. In each case, we obtained very precise values with errors in the range 3%–10% for mass and 2%–8% for radius within $1\sigma$ confidence. We show here that, with the *ATHENA* WFI detector, such a determination could be used to constrain the EOS of superdense neutron star matter.

*Unified Astronomy Thesaurus concepts:* Neutron stars (1108); Compact objects (288); Stellar atmospheres (1584)

## 1. Introduction

Almost 50 years after confirmation of the existence of neutron stars (Hewish et al. 1968), the equation of state (EOS) of the matter that comprises these stars is still under discussion. In neutron stars, the density in the center is a few times the nuclear density. Many theoretical models of the EOS of superdense matter have been proposed (see the extensive review by Haensel et al. 2007). The models have assumed both normal matter and matter in exotic states, like condensates of pions or kaons, superfluid or superconductive matter, or even free quarks. Astronomical observations are the only way to verify the EOS of neutron stars, because in Earth laboratories we are unable to reproduce conditions similar to neutron star interiors. A very important property of theoretical models is the existence of a maximum mass for the neutron star and a unique mass–radius relation for each assumed EOS. There exist multiple methods to constrain the EOS using astronomical observations.

Astronomers seek to discover the heaviest neutron stars (Demorest et al. 2010; Antoniadis et al. 2013). Measurements of the maximum mass allows one to exclude those EOS models that predict a maximum mass lower than the observed maximum. Comparison of both masses does not allow for a unique determination of the EOS. There exist methods that allow for simultaneous determination of mass and radius and, consequently, of the EOS. One such method is fitting of the observed spectra with model atmospheres, but until the necessary high-quality spectra are available, the accuracy of mass and radius determination will remain an open question. We expect that such high-quality spectra can be obtained by the detectors onboard *ATHENA* (Advanced Telescope for High Energy Astrophysics), especially since a growing population of bursters, currently numbered at 110,[4] has been observed by almost every major X-ray satellite (Watts et al. 2016; Galloway & Keek 2017, and references therein).

*ATHENA* is an X-ray mission proposed by the ESA to address the Hot and Energetic Universe science theme (Nandra et al. 2013). The mission will be launched in 2031 and placed at the second Sun–Earth Lagrangian point (L2). The planned mission lifetime is five years, but is expected to be longer. *ATHENA* will be equipped with two scientific instruments: the X-ray Integral Field Unit (X-IFU; Barret et al. 2013) and the Wide Field Imager (WFI; Rau et al. 2013).

The WFI has a large field of view $40'\times40'$, and very high angular resolution, $5''$. It will observe in the energy range 0.2–15 keV with resolution 170 eV at 7 keV. The planned time resolution for this instrument is 80 $\mu$s. It's scientific goals are related to high-energy phenomena, and include studying hot baryons in groups and clusters of galaxies, accretion processes onto compact objects, and gamma-ray bursts and other transient objects. The high time resolution of WFI in combination with the large effective area of the *ATHENA* mirrors make this detector fast enough to be used for studying neutron stars during bursts. Such conditions are needed for mass and radius determination when using the continuum-fitting method.

The continuum-fitting method was first described by Majczyna & Madej (2005). They fit Proportional Counter Array (PCA)/*Rossi X-ray Timing Explorer* (*RXTE*) spectra of MXB 1728−34 taken during a phase between the bursts. Each spectrum was integrated over 16 s. These authors fit numerical models calculated with the ATM21 code to the observed spectra. The same models were fitted to the observed spectra of 4U 1820−30 (Kuśmierek et al. 2011). They obtained values of mass $M = 1.3 \pm 0.6\ M_{\odot}$ and radius $R = 11^{+3}_{-2}$ km, consistent with results obtained by other researchers. Errors in the paper by Kuśmierek et al. (2011) are relatively large but they could

[4] http://burst.sci.monash.edu/sources

be reduced if some systematic effects now known now (e.g., accretion during even strong bursts) are included. Continuum fitting for neutron star mass and radius determination can be also used without complicated calculations of neutron star atmospheres; instead, blackbody emission multiplied by the color correction factor can be assumed (Özel et al. 2009). This approach is faster, but it does not take into account that, in reality, the overall shape of the emitted spectrum is modified by Compton scattering, especially at the hard tail of the spectrum (Majczyna & Madej 2005; Suleimanov et al. 2011).

In our analysis we used fake spectra, therefore we made the principal assumption that our theoretical models are valid for this "source." We do not widely discuss validation of each assumption of our model in the context of real sources, but we note that our theoretical spectra could be used to fit the observed spectra of real sources (see, e.g., Kuśmierek et al. 2011). In this paper, we clearly show that the data that will be provided by *ATHENA*/WFI will allow us to determine mass and radius using the continuum-fitting method, with errors as small as 3%–10% for mass determination and 2%–8% for radius determination even for relatively dim sources.

## 2. The ATM24 Model Code

The model atmospheres and theoretical X-ray spectra of hot neutron stars used in this paper were computed with the ATM24 code, which is the next version of the ATM21 code (Madej 1991; Majczyna et al. 2005) upgraded for numerical precision. The accuracy of the code has been recently demonstrated by Madej et al. (2017) and Vincent et al. (2018). The ATM24 code calculates the radiative transfer equation in a plane-parallel geometry. It takes into account the effect of Compton scattering on free, relativistic electrons, where initial photon energies can approach the electron rest mass. We assume the EOS of an ideal gas being in local thermodynamical equilibrium (LTE). Nevertheless, the Compton scattering redistribution functions of X-ray photons $\Phi(\nu, \nu')$ are fully non-LTE terms of the radiative transfer equation.

The equation of transfer was adopted from Pomraning (1973; see also Sampson 1959). The working equation of transfer and the temperature correction procedure were presented originally by Madej (1989, 1991) and used correctly by Madej et al. (2017) and Vincent et al. (2018). The final equation of transfer is written on the monochromatic optical depth scale $d\tau_\nu = -(k_\nu + \sigma_\nu)\rho\, dz$, and has the form

$$\mu \frac{dI_\nu}{d\tau_\nu} = I_\nu - \frac{k_\nu}{k_\nu + \sigma_\nu} B_\nu - \left(1 - \frac{k_\nu}{k_\nu + \sigma_\nu}\right) J_\nu + \left(1 - \frac{k_\nu}{k_\nu + \sigma_\nu}\right) J_\nu \int_0^\infty \Phi(\nu, \nu') \times \left(1 + \frac{c^2}{2h\nu'^3} J_{\nu'}\right) d\nu' + -\frac{k_\nu}{k_\nu + \sigma_\nu}\left(1 + \frac{c^2}{2h\nu^3} J_\nu\right) \times \int_0^\infty \Phi(\nu, \nu') J_{\nu'} \left(\frac{\nu}{\nu'}\right)^3 \exp\left[-\frac{h(\nu - \nu')}{kT}\right] d\nu', \quad (1)$$

where $k_\nu$ and $\sigma_\nu$ denote coefficients of absorption and electron scattering, respectively. $I_\nu$ is the energy-dependent specific intensity, $J_\nu$ is the mean intensity of radiation, and $z$ is the geometrical depth in the considered atmosphere.

We used the angle-averaged redistribution function $\Phi(\nu, \nu')$ and Compton scattering cross-section $\sigma(\nu \to \nu', \vec{n} \cdot \vec{n'})$, following the method of Guilbert (1981), which was corrected for a computational error by Madej (1991). The Compton redistribution function is related to the cross-section as defined in Madej (1989):

$$\Phi(\nu, \nu') = \frac{1}{\sigma_\nu} \oint_{\omega'} \frac{d\omega'}{4\pi} \sigma(\nu \to \nu', \vec{n} \cdot \vec{n'}). \quad (2)$$

We solve the model atmosphere assuming constraints of hydrostatic and radiative equilibrium. We are aware that for atmospheres in motion this assumption is too strong; however, such models have been widely used to fit X-ray spectra (see, e.g., Medin et al. 2016; Suleimanov et al. 2017). The influences of magnetic field and accretion onto the neutron star are not included. Our code takes into account energy-dependent opacities of hydrogen, helium, and heavy element ions in LTE. The ionization equilibrium is fully solved, allowing for the appearance of iron lines for specific initial parameters (Majczyna et al. 2005). We neglect the effects of electron degeneracy, which are unimportant in the hot atmospheres relevant to our studies. Examples of the theoretical local spectra for one value of effective temperature and several surface gravities are shown in Figure 1. Near the maximum flux, a few emission iron lines are clearly seen.

The right panel of Figure 1 shows spectra of a hot neutron star calculated using the ATM24 code for the same effective temperature $T_{\rm eff} = 2.20 \times 10^7$ K and logarithm of surface gravity from $\log(g) = 14.30$ up to $\log(g) = 14.60$. We assume a pure hydrogen atmosphere. For comparison we also add a spectrum of an atmosphere composed of hydrogen, helium, and iron in the following proportions: $N_{\rm He}/N_{\rm H} = 0.11$ and $N_{\rm Fe}/N_H = 3.7 \times 10^{-5}$, and $\log(g) = 14.40$.

## 3. Simulated Spectrum

*ATHENA* is a future mission; therefore for the aim of this paper, we simulated a spectrum that will be detected by the WFI instrument. We used publicly available calibration files[5] provided by the *ATHENA* mission team. The effective area at 1 keV is 1.4 $m^2$. To simulate the observed spectrum with the WFI detector, we used the "fake" command in the `xspec 12.6.0` fitting package (Arnaud 1996). This command works on theoretical models and simulates the data taking into account *ATHENA*/WFI responses and background files for the newest mirror design with 15 rows[1]. The obtained data file is accompanied by a simulated new background file. In the case of the simulated spectrum and background all errors are Poissonian.

To produce the simulated data, we choose three models with various parameters for the neutron star atmosphere: effective temperature $T_{\rm eff}$, surface gravity $\log(g)$, gravitational redshift $z$, and the normalization factor $N_{\rm ATM}$ given in Table 1. We name those models A, B, and C respectively. The values of $\log(g)$ and $z$ correspond to particular masses and radii of neutron stars given in the table (see Section 5 for the relations between the parameters). The normalization factor is directly related to the ratio of the neutron star radius to distance $D$ as $(R/D)^2$. We normalize our models in such a way that the values of observed fluxes correspond to semi-bright Galactic X-ray sources. All observed fluxes are given in the last row of Table 1.

[5] http://www.mpe.mpg.de/ATHENA-WFI/response_matrices.html

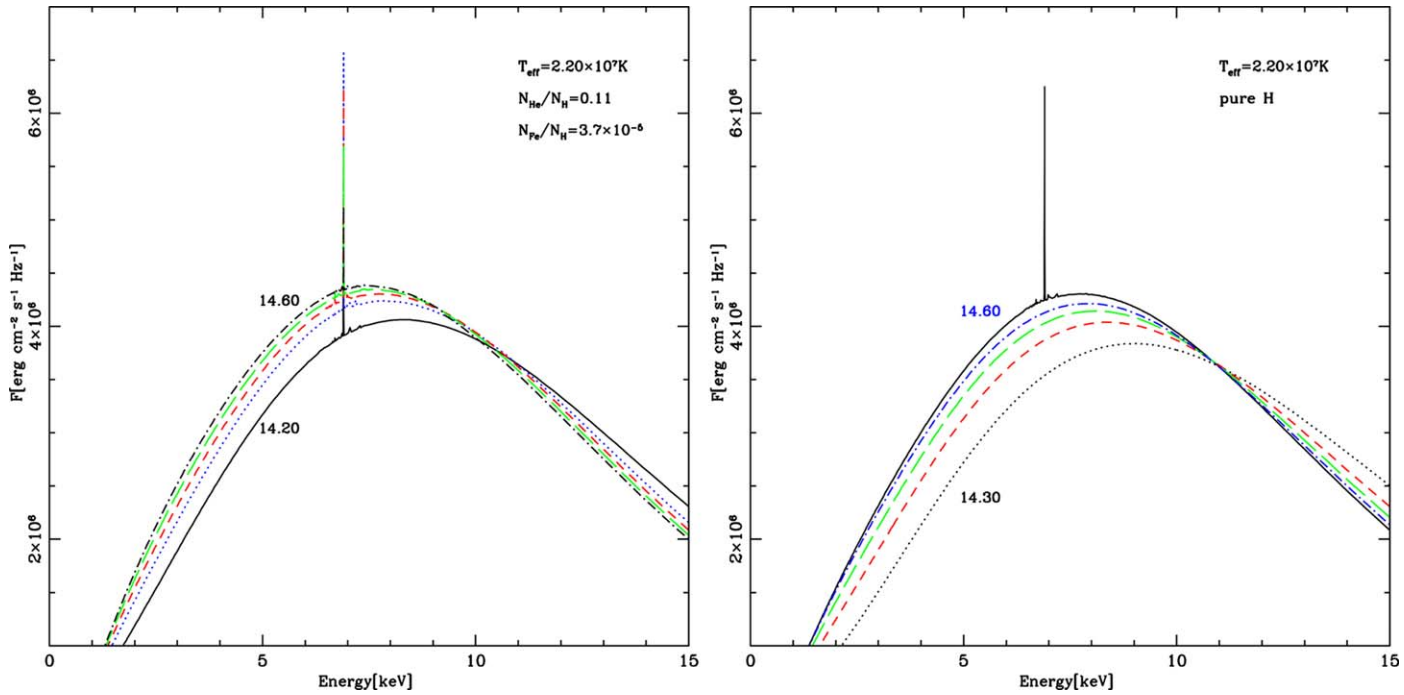


**Figure 1.** Theoretical local spectrum of a hot neutron star atmosphere with parameters $T_{\rm eff} = 2.20 \times 10^7$ K and different surface gravities: left panel from $\log(g) = 14.20$–$14.60$; right panel from 14.30–14.60. The assumed hydrogen–helium–iron composition is of solar proportion in the left panel, and a pure hydrogen atmosphere is assumed in the right panel, where we add a comparison spectrum of an atmosphere with iron and $\log(g) = 14.40$ (solid black line).

**Table 1**
Parameters of the Fake Spectrum for A, B, and C Model Atmospheres: Hydrogen Column Density $N_H$, Effective Temperature $T_{\rm eff}$, Surface Gravity $\log(g)$, Gravitational Redshift $z$, and Normalization Factor $N_{\rm ATM}$

| Name | A | B | C |
|---|---|---|---|
| $N_H$ (cm$^{-2}$) | $0.8 \times 10^{22}$ | $0.8 \times 10^{22}$ | $0.8 \times 10^{22}$ |
| $T_{\rm eff}$ (K) | $2.19 \times 10^7$ | $2.20 \times 10^7$ | $2.21 \times 10^7$ |
| $\log(g)$ (cgs) | 14.25 | 14.30 | 14.35 |
| $z$ | 0.240 | 0.300 | 0.350 |
| $N_{\rm ATM}$ | $2.5 \times 10^{-24}$ | $2.5 \times 10^{-24}$ | $2.5 \times 10^{-24}$ |
| $M$ ($M_\odot$) | 1.297 | 1.653 | 1.869 |
| $R$ (km) | 10.956 | 11.954 | 12.230 |
| $F$ (erg cm$^{-2}$ s$^{-1}$) | $4.51 \times 10^{-10}$ | $4.42 \times 10^{-10}$ | $4.32 \times 10^{-10}$ |

**Note.** In the last three rows we display corresponding masses, radii, and fluxes for those sources.

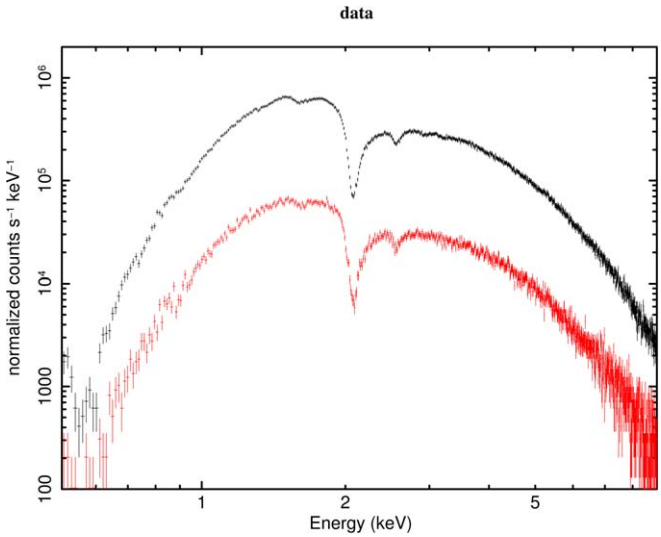


**Figure 2.** Simulated WFI spectra for arbitrarily chosen parameters: $T_{\rm eff} = 2.2 \times 10^7$K, $\log(g) = 14.3$, $z = 0.30$, and $N_{\rm ATM} = 2.5 \times 10^{-24}$ (fake spectrum B; black crosses) and $N_{\rm ATM} = 2.5 \times 10^{-25}$ (red). Systematic errors at the level of 3% are taken into account. The chemical composition is assumed as a mixture of hydrogen, helium, and iron in solar proportions. The time exposure $t_{\rm exp}$ is equal to 1 s. The overall data are shaped by the *ATHENA* mirrors and WFI effective area.

These parameters are not related to any particular existing neutron star, but compact objects with these parameters certainly could be realized in nature. The chemical composition is assumed as a mixture of hydrogen $N_{\rm He}/N_{\rm H} = 0.11$ and iron $N_{\rm Fe}/N_{\rm H} = 3.7 \times 10^{-5}$ (number abundances). Corresponding relative mass abundances are $M_{\rm H} = 0.6950$, helium $M_{\rm He} = 0.3035$, and iron $M_{\rm Fe} = 1.425 \times 10^{-3}$. Finally all our models are multiplied by an interstellar absorption model (TBABS in `xspec`) with the same assumed hydrogen column density $N_{\rm H} = 0.80 \times 10^{22}$ cm$^{-2}$. We set the time exposure $t_{\rm exp}$ equal to 1 s. This value of $t_{\rm exp}$ can be used for objects like isolated neutron stars or X-ray transients in the period when the neutron star is not accreting matter.

In the case of X-ray bursters, however, the situation is more complicated. In such objects the method based on fitting observed spectra should be used for photospheric radius expansion bursts in the touchdown phase in the hard state. In such a situation the exposure time should be much shorter, of the order of tenths of a second. Therefore only very sensitive detectors with large effective area and time resolution of the order of microseconds can be used. In the past, the best observational spectra were provided by the *RXTE* which allowed collection of many counts over 0.1 s. The CCD-type detectors used onboard *Chandra* and *XMM-Newton* are not fast enough to collect a sufficient amount of photons even during the maximum burst phase. Therefore, the fitting procedure of continuum emission for mass and radius determination would

**Table 2**
Best-fit Parameters and $1\sigma$ and $2\sigma$ Errors (in Parentheses)

| $N_H$ | | log($g$) | | z | | $M$ ($M_\odot$) | | $R$ (km) | |
|---|---|---|---|---|---|---|---|---|---|
| | | | | Fake Spectrum A | | | | | |
| 0.802 | $^{+0.002}_{-0.002}(^{0.004}_{0.004})$ | 14.26 | $^{+0.03}_{-0.02}(^{+0.03}_{-0.03})$ | 0.255 | $^{+0.005}_{-0.020}(^{+0.020}_{-0.025})$ | 1.40 | $^{+0.05}_{-0.15}(^{+0.20}_{-0.24})$ | 11.32 | $^{+0.32}_{-0.94}$ $(^{+1.24}_{-1.32})$ |
| | | | | Fake Spectrum B | | | | | |
| 0.804 | $^{+0.002}_{-0.002}(^{0.004}_{0.004})$ | 14.28 | $^{+0.04}_{-0.0005}(^{+0.06}_{-0.01})$ | 0.305 | $^{+0.015}_{-0.010}(^{+0.025}_{-0.015})$ | 1.78 | $^{+0.05}_{-0.13}(^{+0.18}_{-0.25})$ | 12.71 | $^{+0.19}_{-0.95}(^{+0.87}_{-1.64})$ |
| | | | | Fake Spectrum C | | | | | |
| 0.800 | $^{+0.002}_{-0.002}(^{0.004}_{0.003})$ | 14.32 | $^{+0.04}_{-0.02}(^{+0.06}_{-0.03})$ | 0.360 | $^{+0.015}_{-0.015}(^{+0.030}_{-0.025})$ | 2.09 | $^{+0.15}_{-0.22}(^{+0.24}_{-0.31})$ | 13.44 | $^{+0.99}_{-1.08}(^{+1.32}_{-1.88})$ |

**Table 3**
Best-fit Parameters for Our Three Fake Spectra, A, B, and C (Confidence Values for $1\sigma$, $2\sigma$, and $3\sigma$ Are Given in the Next Three Rows for Each Model)

| | $z$ | log($g$) (cgs) | $M$ ($M_\odot$) | $R$ (km) |
|---|---|---|---|---|
| | | Fake Spectrum A | | |
| Best Par. | 0.255 | 14.26 | 1.399 | 11.315 |
| $1\sigma$ | 0.235–0.260 | 14.24–14.29 | 1.252–1.444 | 10.371–11.637 |
| $2\sigma$ | 0.230–0.275 | 14.23–14.29 | 1.155–1.595 | 9.992–12.556 |
| $3\sigma$ | 0.220–0.258 | 14.22–14.31 | 1.049–1.711 | 9.392–13.068 |
| | | Fake Spectrum B | | |
| | $z$ | log($g$) (cgs) | $M$ ($M_\odot$) | $R$ (km) |
| Best Par. | 0.305 | 14.28 | 1.776 | 12.705 |
| $1\sigma$ | 0.295–0.320 | 14.28–14.32 | 1.647–1.825 | 11.758–12.892 |
| $2\sigma$ | 0.290–0.330 | 14.27–14.34 | 1.531–1.959 | 11.066–13.573 |
| $3\sigma$ | 0.280–0.335 | 14.26–14.35 | 1.429–2.054 | 10.494–14.083 |
| | | Fake Spectrum C | | |
| | $z$ | log($g$) (cgs) | $M$ ($M_\odot$) | $R$ (km) |
| Best Par. | 0.360 | 14.32 | 2.090 | 13.437 |
| $1\sigma$ | 0.345–0.375 | 14.30–14.36 | 1.869–2.235 | 12.230–14.243 |
| $2\sigma$ | 0.335–0.390 | 14.29–14.38 | 1.782–2.334 | 11.558–14.752 |
| $3\sigma$ | 0.325–0.395 | 14.28–14.40 | 1.630–2.486 | 10.761–15.456 |

not be very precise for data from those satellites. Besides the case of X- ray bursters presented in this paper, our method could also be used for isolated neutron stars or transient objects. However, for different sets of physical parameters, new model computations would be required.

Since our analysis relies on X-ray spectra, systematic errors can be important (Arnaud et al. 2011; Lee et al. 2011; Xu et al. 2014). In order to place constraints on the parameters from the spectral shape (as in the case of our paper), only relative area on-axis systematic errors are important, which influence the observed spectral shape, and therefore estimation of model parameters (in our case neutron star mass and radius). Those errors depend on the detector calibration and for *ATHENA* the expected value is at the level of 3% (*ATHENA* calibration requirement document, ESA Technical Note). Therefore, after our fake spectra were made, we added systematic errors on the level of 3% using the `xspec` ftool GRPPHA.

Figure 2 shows two simulated spectra for parameters of model B and two different assumed unabsorbed fluxes - $f_{2-10\,\mathrm{keV}} = 4.42 \times 10^{-10}$ erg cm$^{-2}$ s$^{-1}$ (black crosses) and $f_{2-10\,\mathrm{keV}} = 4.41 \times 10^{-11}$ erg cm$^{-2}$ s$^{-1}$ (red). For the spectrum with larger flux, for a 1 s exposure time, we collected $2.36 \times 10^6$ photons, enough to achieve our science goal.

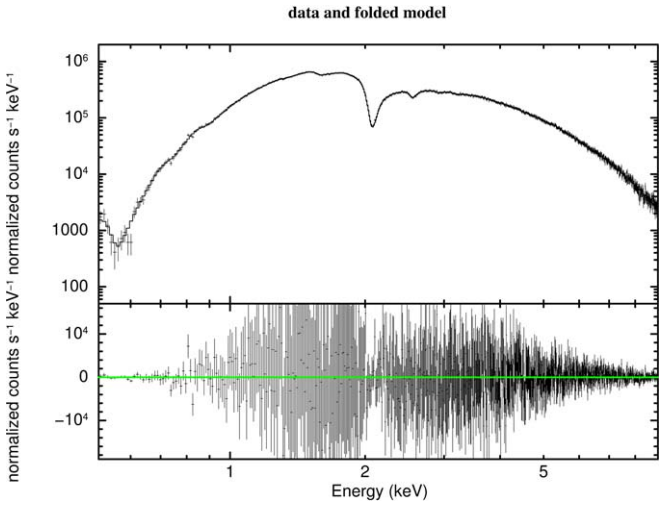


**Figure 3.** Top panel: data (fake spectrum B) and our best-fit model; bottom panel: residua (data minus the folded model). Parameters of the fit are $T_{\mathrm{eff}} = 2.18 \times 10^7$K, log($g$) = 14.28, $z = 0.305$, $N_{\mathrm{ATM}} = 2.56 \times 10^{-24}$, and $N_{\mathrm{H}} = 0.804 \times 10^{22}$ cm$^{-2}$; $\chi^2 = 518.52/869$.

## 4. Fitting Procedures.

Our method of determination of neutron star parameters is based on the fitting of theoretical spectra to the observed one, in this case to the *ATHENA*/WFI fake spectrum. We use the fake data with higher unabsorbed flux (black crosses at Figure 2) for further analysis.

The theoretical models used to fit the fake spectrum are constructed for one chemical composition, given above. Four parameters, effective temperature, surface gravity, gravitational redshift, and normalization, are free parameters in our fitting procedure. In addition, $T_{\mathrm{eff}}$ and log ($g$) are input parameters in our atmospheric ATM24 numerical simulations. We calculated an extensive grid of theoretical spectra (nearly 5000 models) with the chemical composition given above. In our initial grid of models, the effective temperature ranges from $10^7$ K to $2.70 \times 10^7$ K with step $\Delta T_{\mathrm{eff}} = 0.02 \times 10^7$K, and surface gravity log ($g$) from the critical value up to 15.0 (cgs) with $\Delta\log(g) = 0.02$. However, we found that the error in log ($g$) is smaller than $\Delta\log(g) = 0.02$, so it was obvious that we needed a denser grid of models. Thus, we chose smaller parameter steps around our reference values for effective temperature and gravity. For effective temperatures in the range from $T_{\mathrm{eff}} = 2.18 \times 10^7$ K to $2.22 \times 10^7$ K the steps were $\Delta T_{\mathrm{eff}} = 0.01 \times 10^7$ K, and for surface gravity ranging from log ($g$) = 13.9 to 14.60 we chose $\Delta\log(g) = 0.01$. All our models were converted to FITS format (Wells et al. 1981),

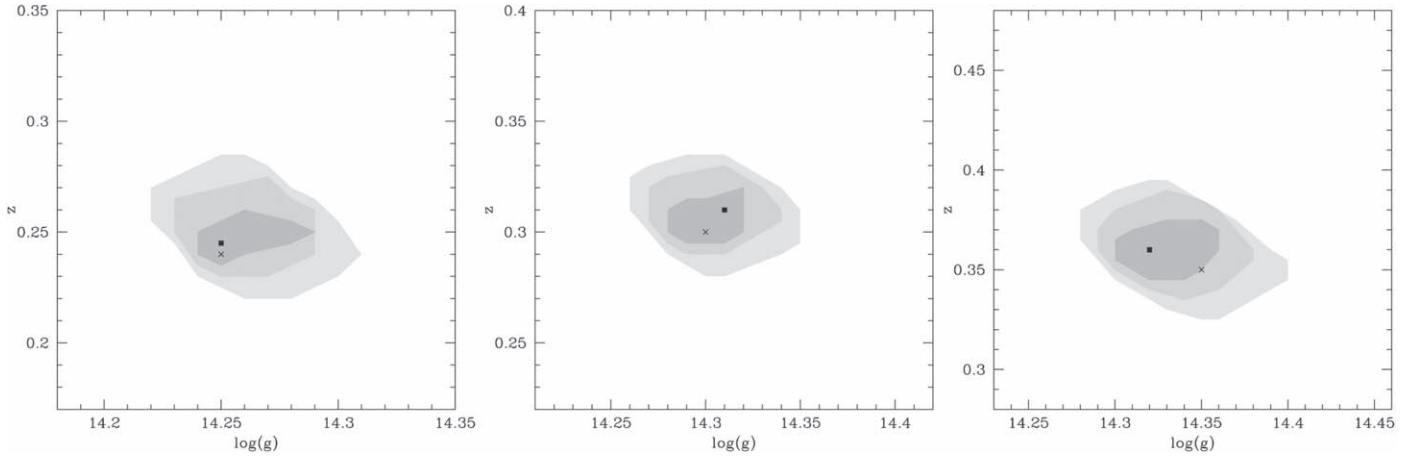


**Figure 4.** $1\sigma$–$3\sigma$ confidence contours for two free parameters, redshift and surface gravity, for model A (left), B (middle), and C (right). The black cross denotes our reference values; the black dot is the best-fit value.

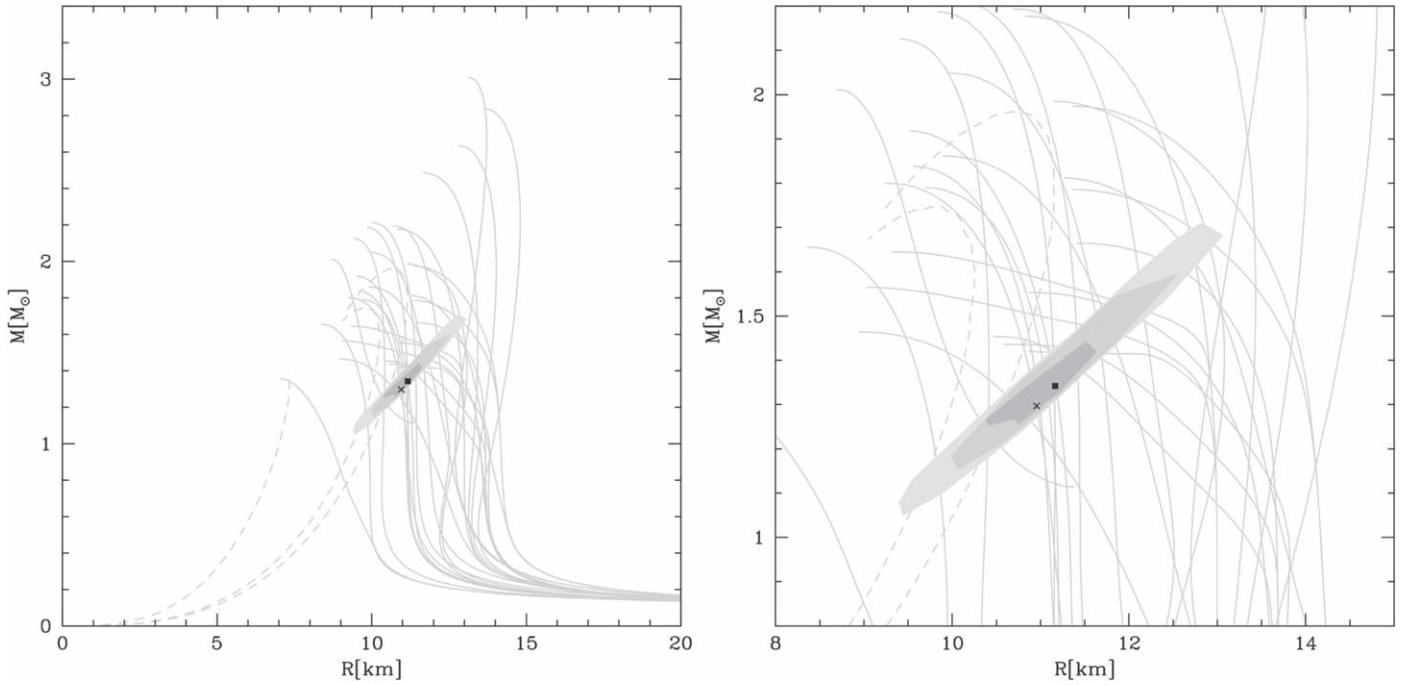


**Figure 5.** $1\sigma$–$3\sigma$ confidence contours for two free parameters, mass and radius, for model A. The right panel is an enlarged version of the left. The black point denotes our best-fit mass and radius values $M = 1.399\,M_{\odot}$ and $R = 11.315$ km; the black cross denotes our reference values. The thin gray lines represent possible EOS solutions (Haensel et al. 2007).

suitable for the `xspec 12.6.0` package (Arnaud 1996). This software was used also to fit our models to the simulated *ATHENA*/WFI spectrum.

For each given combination of values of $T_{\rm eff}$ and $\log(g)$, the surface redshift $z$ was varied from 0.1 to 0.6 in steps of 0.005. The value of $N_{\rm ATM}$ corresponding to the best fit was determined. During the fitting procedure the value of hydrogen column density ($N_H$) in the model of Galactic absorption (TBABS in `xspec`) was a free parameter. Therefore, we obtained a large, five-dimensional table of $\chi^2$ for one assumed chemical composition. From this table, we extracted one set of four parameters ($T_{\rm eff}$, $\log(g)$, $z$, and $N_{\rm ATM}$) corresponding to the fit with the lowest value of $\chi^2$. We found also $1\sigma$, $2\sigma$, and $3\sigma$ confidence levels in $\log(g) - z$ parameter space, requiring that $\chi^2_{\rm min} < \chi^2 < \chi^2_{\rm min} + \Delta\chi^2$, and additionally that $0.1 < M < 3M_{\odot}$. The value of $\Delta\chi^2$ corresponds to the $1\sigma$, $2\sigma$, and $3\sigma$ confidence levels for two free parameters (Press et al. 1992). The best-fit model and residua are presented in Figure 3.

## 5. Results

As a result of fitting the simulated *ATHENA*/WFI data we determined the effective temperature $T_{\rm eff}$, surface gravity $\log(g)$ and gravitational redshift $z$. The last two parameters are converted into mass and radius of the neutron star following Majczyna & Madej (2005):

$$R = \frac{zc^2}{2g}\frac{(2+z)}{(1+z)}, \tag{3}$$

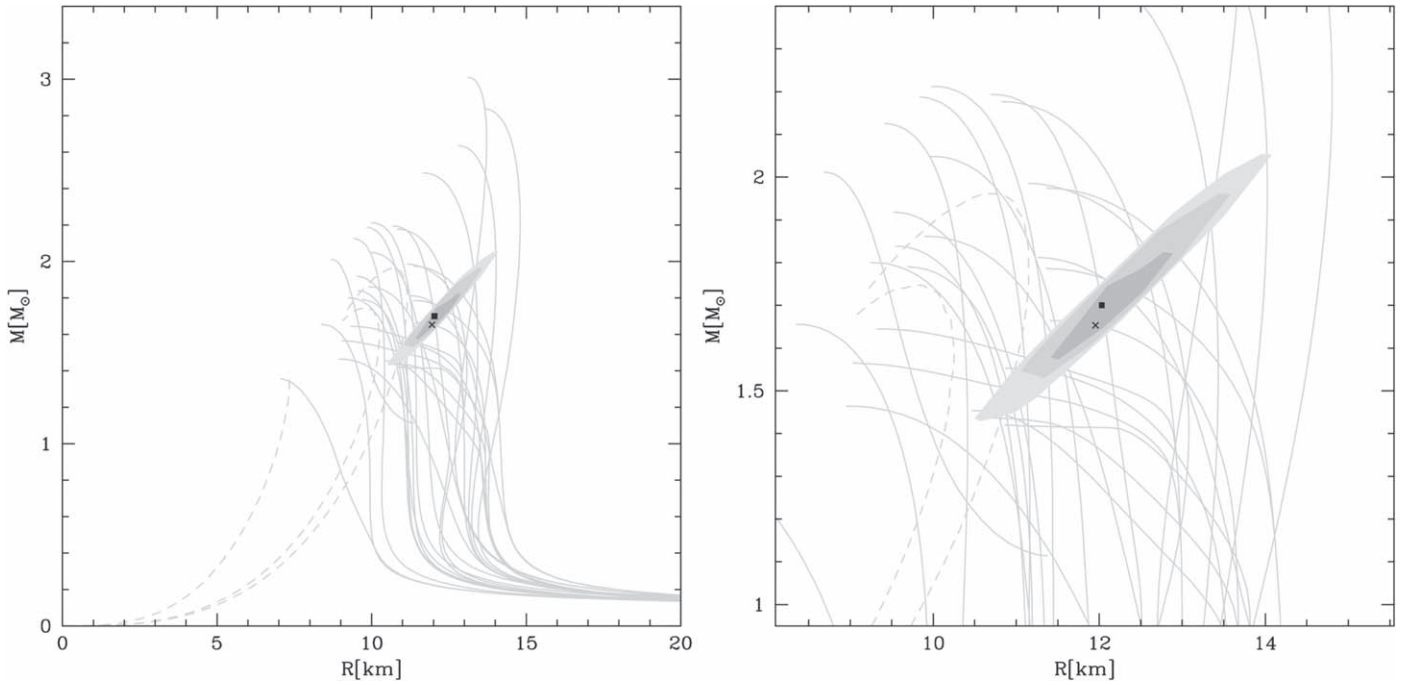


**Figure 6.** $1\sigma$, $2\sigma$ and $3\sigma$ confidence contours for two free parameters: mass and radius for model B. Right panel is the enlarged version of the left panel. The black point denotes our best-fit mass and radius values $M = 1.776\ \mathrm{M}_{\odot}$ and $R = 12.705$ km, whereas the black cross denotes our reference values. The thin grey lines represent possible EOS solutions (Haensel et al. 2007).

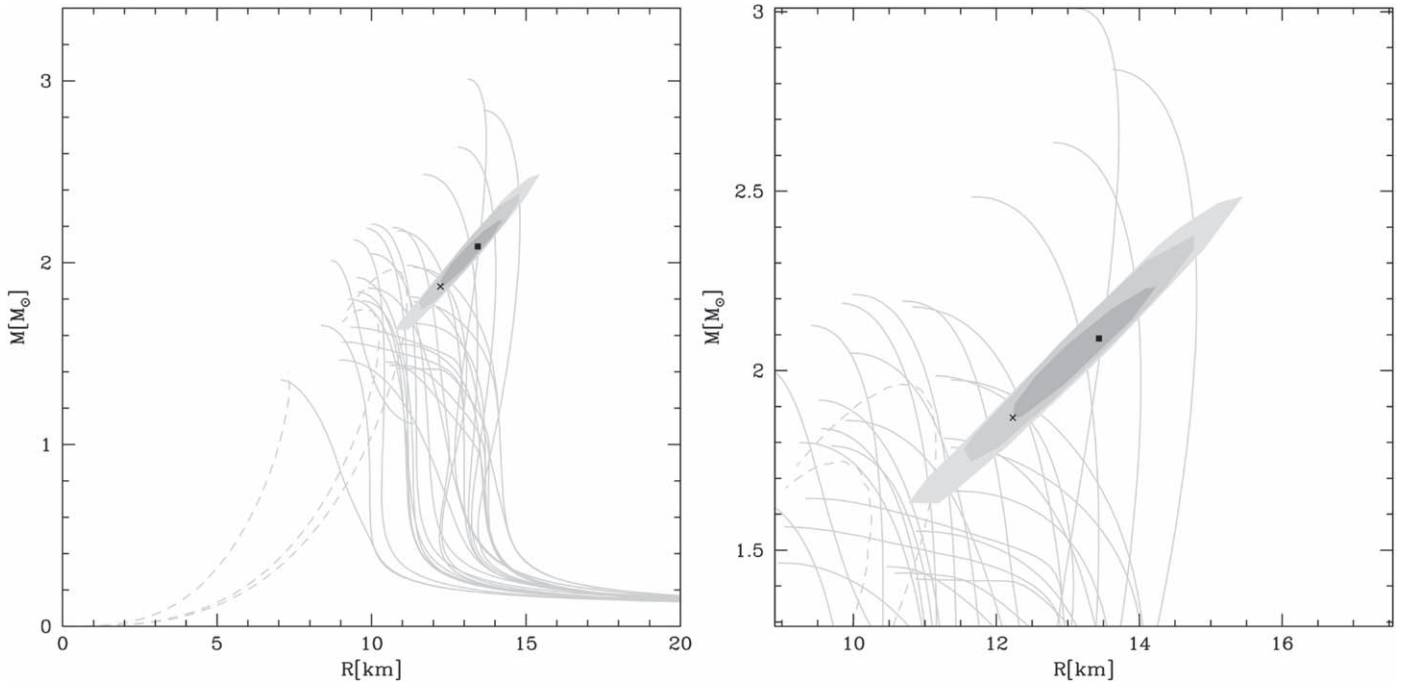


**Figure 7.** $1\sigma$–$3\sigma$ confidence contours for two free parameters, mass and radius, for model C. The right panel is an enlarged version of the left. The black point denotes our best-fit mass and radius values $M = 2.090\ M_{\odot}$ and $R = 13.437$ km; the black cross denotes our reference values. The thin gray lines represent possible EOS solutions (Haensel et al. 2007).

and

$$M = \frac{z^2 c^4}{4gG} \frac{(2+z)^2}{(1+z)^3}, \tag{4}$$

where $G$ is the gravitational constant and $c$ is the speed of light.

Table 2 contains our best-fit parameters and the accuracy of their determination obtained using our method. Errors were defined as $1\sigma$ and $2\sigma$ standard deviations (in parenthesis). The goal of our fitting procedure is to reproduce assumed values of the parameters for which the fake spectrum was calculated (see Section 3). We obtained best-fit parameters that differ slightly from the assumed values, but the difference was less than $1\sigma$ standard deviations. Values of $1\sigma$, $2\sigma$, and $3\sigma$ confidence ranges determined for two free parameters are presented in

Table 3, where the minimum $\chi^2$ corresponds to parameters of the neutron star that differ slightly from the assumed values

Figure 4 shows the $1\sigma$, $2\sigma$, and $3\sigma$ confidence contours are obtained for two free parameters, redshift and surface gravity, for all models. On this figure, the black cross denotes the best-fit value of those parameters. The input assumed values are denoted as a black dot. In all cases, fitted values are within $1\sigma$ confidence contours. Corresponding masses and radii for models A–C are presented in Figures 5–7, respectively. The grey lines denote possible EOS solutions in those figures.

## 6. Summary

Determination of the basic parameters of neutron stars is very important for the derivation of the EOS of superdense matter. In this paper, we presented a method of mass and radius determination for neutron stars. Our method is based on the fitting of theoretical spectra to the observed one. Importantly, our method is independent of distance, which is proportional to the normalization of the model. This is because the normalization factor $N_{\rm ATM}$ is the result of our fitting procedure. Therefore, knowledge of the distance to the source is not necessary with our method. Figure 1 shows our theoretical spectra for two very different chemical compositions. The shapes of the continua of these spectra are different, as well as the locations of their maxima. Those differences indicate that even tentative knowledge of the chemical composition is crucial for our method. For many neutron stars the chemical composition of their atmospheres is known (e.g., Goodwin et al. 2019).

We calculated a large grid of theoretical spectra of hot neutron stars using the ATM24 code, assuming an effective temperatures $T_{\rm eff} = (1.5 - 2.7) \times 10^7$K, logarithm of gravity from 15.0 down to the critical value, and chemical abundances as defined in Section 4. Parameters of models in the grid changed in steps of $\Delta T_{\rm eff} = 0.02 \times 10^7$ K and $\Delta \log(g) = 0.02$; chemical composition was kept the same for all models.

Our goal was to determine the precision of mass and radius determination of neutron stars based on spectra to be obtained with the *ATHENA*/WFI instrument. Due to a lack of real *ATHENA* observations, we simulated three spectra using publicly available WFI calibration files. We constructed three fake spectra A–C corresponding to three different values of effective temperature, surface gravity, and redshift. We chose normalization factors $N_{\rm ATM}$ corresponding to the observed fluxes of a few hundredths of the Crab ($\sim 10^{-10}$erg cm$^{-2}$ s$^{-1}$). *ATHENA* instrument systematic errors at the level of 3% were taken into account where simulated spectra were created.

Next, we fitted these fake spectra with a large grid of our theoretical spectra. We obtained the best fit ($1\sigma$) for the following parameters of the fake spectra: A: $M = 1.40^{+0.05}_{-0.15} M_\odot$ and $R = 11.32^{+0.32}_{-0.94}$ km, B: $M = 1.78^{+0.05}_{-0.13} M_\odot$ and $R = 12.71^{+0.19}_{-0.95}$ km, C: $M = 2.09^{+0.15}_{-0.22} M_\odot$ and $R = 13.44^{+0.99}_{-1.08}$ km, and the corresponding masses and radii for $3\sigma$ confidence ranges $M = 1.05 - 1.71 M_\odot$ and $R = 9.38 - 13.07$ km, $M = 1.43 - 2.05 M_\odot$ and $R = 10.49 - 14.08$ km, $M = 1.63 - 2.49 M_\odot$ and $R = 10.76 - 15.46$ km, respectively.

In each case we determined the precision of the measurements with errors in the range 3%–10% for mass and 2%–8% for radius within $1\sigma$ confidence. All errors ($1\sigma$) are relatively small for the *ATHENA*/WFI detector. We note that the errors defined by $2\sigma$ confidence ranges are in the range 11%–17%. Therefore, we demonstrated that our method will allow one to constrain the EOS of the dense matter of neutron stars using future observations of the *ATHENA* mission.

Special thanks go to Alex Markowitz for helpful discussion and editorial corrections, and to Jan-Willem der Herder and Jorn Wilms for the discussion on systematic errors in the *ATHENA* mission. This work was supported by grants 2015/17/B/ST9/03422 and 2015/18/M/ST9/00541 from the Polish National Science Center.

## ORCID iDs

Agnieszka Majczyna https://orcid.org/0000-0003-0864-8779
Jerzy Madej https://orcid.org/0000-0001-8417-1509
Mirosław Należyty https://orcid.org/0000-0003-0478-5426
Agata Różańska https://orcid.org/0000-0002-5275-4096

## References

Antoniadis, J., Freire, P. C. C., Wex, N., et al. 2013, Sci, 340, 448
Arnaud, K., Smith, R., & Siemiginowska, A. 2011, Handbook of X-ray Astronomy (Cambridge: Cambridge Univ. Press)
Arnaud, K. A. 1996, in ASP Conf. Ser. 101, Astronomical Data Analysis Software and Systems V, ed. V. Systems, G. H. Jacoby, & J. Barnes (San Francisco, CA: ASP), 17
Barret, D., den Herder, J. W., Piro, L., et al. 2013, arXiv:1308.6784
Demorest, P. B., Pennucci, T., Ransom, S. M., Roberts, M. S. E., & Hessels, J. W. T. 2010, Natur, 467, 1081
Galloway, D. K., & Keek, L. 2017, arXiv:1712.06227
Goodwin, A. J., Galloway, D. K., & in't Zand, J. J. M. 2019, MNRAS, 486, 4149
Guilbert, P. W. 1981, MNRAS, 197, 451
Haensel, P., Potekhin, A. Y., & Yakovlev, D. G. 2007, Neutron Stars I: Equation of State and Structure (New York: Springer)
Hewish, A., Bell, S. J., Pilkington, J. D. H., Scott, P. F., & Collins, R. A. 1968, Natur, 217, 709
Kuśmierek, K., Madej, J., & Kuulkers, E. 2011, MNRAS, 415, 3344
Lee, H., Kashyap, V. L., van Dyk, D. A., et al. 2011, ApJ, 731, 126
Madej, J. 1989, ApJ, 339, 386
Madej, J. 1991, ApJ, 376, 161
Madej, J., Różańska, A., Majczyna, A., & Należyty, M. 2017, MNRAS, 469, 2032
Majczyna, A., & Madej, J. 2005, AcA, 55, 349
Majczyna, A., Madej, J., Joss, P. C., & Różańska, A. 2005, A&A, 430, 643
Medin, Z., von Steinkirch, M., Calder, A. C., et al. 2016, ApJ, 832, 102
Nandra, K., Barret, D., Barcons, X., et al. 2013, arXiv:1306.2307
Özel, F., Güver, T., & Psaltis, D. 2009, ApJ, 693, 1775
Pomraning, G. C. 1973, The Equations of Radiation Hydrodynamics (Oxford: Pergamon Press)
Press, W. H., Teukolsky, S. A., Vetterling, W. T., & Flannery, B. P. 1992, Numerical Recipes in FORTRAN. The Art of Scientific Computing (Cambridge: Cambridge Univ. Press)
Rau, A., Meidinger, N., Nandra, K., et al. 2013, arXiv:1308.6785
Sampson, D. H. 1959, ApJ, 129, 734
Suleimanov, V., Poutanen, J., & Werner, K. 2011, A&A, 527, A139
Suleimanov, V. F., Kajava, J. J. E., Molkov, S. V., et al. 2017, MNRAS, 472, 3905
Vincent, F. H., Bejger, M., Różańska, A., et al. 2018, ApJ, 855, 116
Watts, A. L., Andersson, N., Chakrabarty, D., et al. 2016, RvMP, 88, 021001
Wells, D. C., Greisen, E. W., & Harten, R. H. 1981, A&AS, 44, 363
Xu, J., van Dyk, D. A., Kashyap, V. L., et al. 2014, ApJ, 794, 97